AFRL-AFOSR-UK-TR-2012-0045

Tunable Superconducting Split Ring Resonators

Dr. Horst Rogalla

University of Twente
Department of Science and Technology
Building Hogekamp (45)
Enschede, Netherlands 7522 NB

EOARD Grant 08-3026

Report Date: September 2012

Final Report for 01 August 2008 to 31 December 2011

Air Force Research Laboratory
Air Force Office of Scientific Research
European Office of Aerospace Research and Development
Unit 4515 Box 14, APO AE 09421

REPORT DOCUMENTATION PAGE

Form Approved OMB No. 0704-0188

1. REPORT DATE *(DD-MM-YYYY)*	2. REPORT TYPE	3. DATES COVERED *(From – To)*
19 September 2012	Final Report	1 August 2008 – 31 December 2011

4. TITLE AND SUBTITLE

Tunable Superconducting Split Ring Resonators

5a. CONTRACT NUMBER

FA8655-08-1-3026

5b. GRANT NUMBER

Grant 08-3026

5c. PROGRAM ELEMENT NUMBER

61102F

6. AUTHOR(S)

Dr. Horst Rogalla

5d. PROJECT NUMBER

5d. TASK NUMBER

5e. WORK UNIT NUMBER

7. PERFORMING ORGANIZATION NAME(S) AND ADDRESS(ES)

University of Twente
Department of Science and Technology
Building Hogekamp (45)
Enschede, Netherlands 7522 NB

8. PERFORMING ORGANIZATION REPORT NUMBER

N/A

9. SPONSORING/MONITORING AGENCY NAME(S) AND ADDRESS(ES)

EOARD
Unit 4515 BOX 14
APO AE 09421

10. SPONSOR/MONITOR'S ACRONYM(S)

AFRL/AFOSR/RSW (EOARD)

11. SPONSOR/MONITOR'S REPORT NUMBER(S)

AFRL-AFOSR-UK-TR-2012-0045

12. DISTRIBUTION/AVAILABILITY STATEMENT

Approved for public release; distribution is unlimited. (approval given by local Public Affairs Office)

13. SUPPLEMENTARY NOTES

14. ABSTRACT

The following phases were targeted for this project: (1) calculation and numerical simulation of a Josephson-inductance tuned HTS ring-resonator and an array for negative index material applications, (2) fabrication of single resonator structures with integrated Josephson tuning and control lines; measurement of the basic features of such resonators, (3) measurement of microwave properties of a single resonator, such as quality factor, tuning range, microwave field-strength distortion and quality-factor dependence on tuning. Feedback for changes in design and fabrication, (4) design and fabrication of arrays of tunable resonators, and (5) testing for microwave properties and negative index operation.
The report continues with a section on the results obtained in the manufacturing of passive high –Tc SSRRs, followed by a section about the properties of the realized SRRs and finally by describing how to ad Josephson junction devices in the resonator structure for the purpose of tuning. The specific challenges in this regard are also mentioned.

15. SUBJECT TERMS

EOARD, high temperature superconductors, Superconductivity

16. SECURITY CLASSIFICATION OF:			17. LIMITATION OF ABSTRACT	18, NUMBER OF PAGES	19a. NAME OF RESPONSIBLE PERSON
a. REPORT	b. ABSTRACT	c. THIS PAGE			SCOTT DUDLEY, Lt Col, USAF
UNCLAS	UNCLAS	UNCLAS	SAR	19	**19b. TELEPHONE NUMBER** *(Include area code)* +44 (0)1895 616162

Tunable Superconducting Split Ring Resonators

H. Rogalla, A. Andreski, F. Tang

Final Report for Project FA8655-08-1-3026

1 Introduction

A split-ring resonator (SRR) is a passive device made of a non-magnetic conducting material, typically a structured thin film on a solid substrate, and intended to resonantly interact with the magnetic component of electromagnetic waves with a wavelengths much greater than the size of the SRR. The last property allows periodic arrays of such resonators to behave as a homogenous (electro)magnetic medium since, from the perspective of incident waves, the size of the individual components of the array will be negligibly small. This on the other hand opens up the possibility to "engineer" the effective permeability μ_{eff} of such artificial material - in a given frequency range - by choosing the type and size of the structure used for the individual SRR elements in the array [1]. Most interesting are those values of the EM constants which are either rare or non-occurring in natural media, such as for instance $\epsilon_{eff} = \mu_{eff} = -1$: a material with a negative index of refraction (ϵ_{eff} can also be "engineered" with an array of resonant structures but of a different type). The most potent and immediate application of these meta-materials is found in RF optics (antennae etc.) where considerable improvements in both size and performance over standard elements can be achieved. It is also important to note that an SRR array is in fact a magnetically active medium (i.e. $\mu_{eff} \neq 1$) although none of the used materials have that property.

Due to the resonant nature of the SRR's interaction with EM waves, the "engineering" of the effective EM constants can occur only inside a small frequency range. The width of the frequency range in resonant interactions is typically proportional to the ratio between the energy lost (dissipated) and the energy exchanged between the interacting elements per period (this ratio also named the Quality-factor Q). In order to obtain a sharp frequency response of the artificial medium, necessary for a good frequency selectivity in practical applications, one must minimize the dissipation in the SRR materials: both in the conductive layer as well as in the substrate. It is then obvious that an SRR built with a superconducting material on a low-loss substrate results in reduced dissipation and consequently better selectivity. Here we report on SRRs made by using the high-T_c cuprate superconductor YBCO ($T_c \approx 90K$) deposited on an oxide substrate MgO. The intrinsically high Q of superconducting resonators can easily be adjusted to lower values (e.g. to increase the bandwidth) by adding controlled dissipative elements.

For many applications tuning of the resonance frequency of the SRR is needed. Classically this is done by varactor diodes. Their capacitance can

be changed by a voltage bias, resulting in an unwanted change of their effective resistance and thus of the Q of the SRR. If superconductors are used for the resonators, one can apply Josephson junctions for tuning the resonance frequency of an SRR, using the supercurrent dependent (Josephson) inductance of a Josephson junction. Josephson junction-based devices are very sensitive to control signals in the (static) magnetic domain, avoiding voltage bias/control typically found in conventional active semiconductor devices and the associated dissipative losses therein. This way an almost dissipationless active superconducting circuit with magnetic control signals can be incorporated in an otherwise passive superconducting SRR (SSRR) structure for the purpose of tunability. The control can be very fast so that also fast adjustments to a changing electromagnetic environment can be realized or active frequency control as needed for fast frequency hopping. An array of these active SSRRs will thus behave as an EM medium of externally controllable effective dielectric and magnetic constants. Note that the properties of the medium can only be controlled by one or a few percent in reality, dependent on the operating frequency.

The report continues with a section on the results obtained in the manufacturing of passive high-T_C SSRRs, followed by a section about the properties of the realized SRRs and finally by describing how to add Josephson junction devices in the resonator structure for the purpose of tuning. The specific challenges in this regard are also mentioned.

2 Basics and Manufacturing of High-T_c SSRRs

A typical (single) split-ring resonator structure is depicted in Figure 1. It consists of a circular or rectangular ring which is opened in one place. This allows for a combination of the inductance of the ring structure with the capacitance of the gap to form a resonator circuit. The advantage of such a circuit is its quite low resonance frequency compared to other structures of similar size.

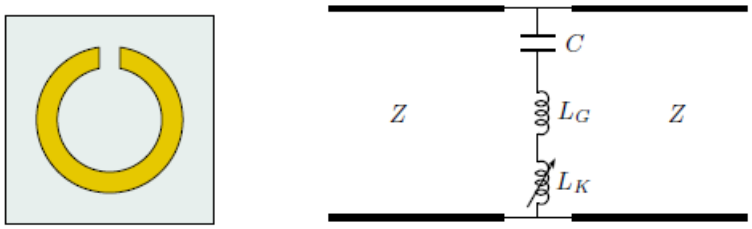

Figure 1: A schematic SSRR (left) and an equivalent circuit (right). C is the gap and surface capacitance, L_GC is the magnetic (geometrical) inductance of the ring and L_K the temperature dependent kinetic inductance of the superconductor.

Different versions of SSRs are being used, often one adds a second concentric split-ring rotated by 180°. This double split-ring resonator structure is depicted in Figure 2. Two tightly concentric rings are interrupted along their length, these gaps placed on opposite sides of the two rings. The purpose of the gap is to stop currents induced by an incident magnetic field (normal to the plane) from closing along any single ring. Due to the strong capacitive coupling along the

edges of the two rings, the induced (RF) currents will however be able to close the gap by distributing through the coupled edges and then flowing through the other ring adjacent to the gap. The process is schematically illustrated in Figure 2 as well.

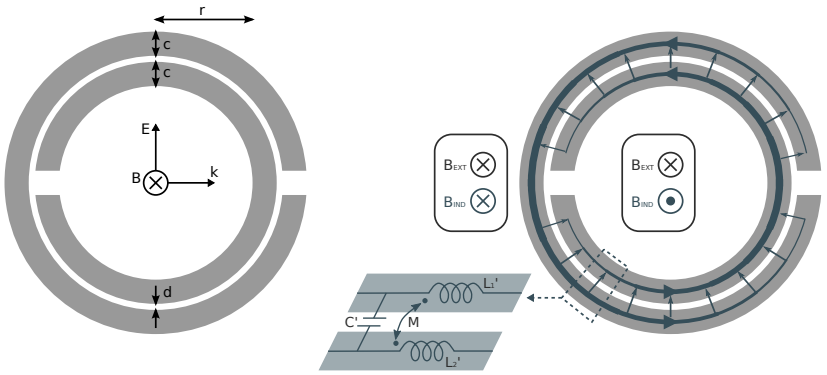

Figure 2: A drawing of the typical SRR (left) and the $L-C$ coupling mechanism allowing induced RF currents to circulate around the structure (right). Note how the induced current counteracts the field inside the rings while adding to it outside.

If the gaps were closed and hence currents were allowed to freely circulate along the rings, one would obtain an ideal diamagnetic response ($\mu_r = -1$) within the area enclosed by the rings as the external flux will be exactly counteracted by the induced currents. Outside the ring area however the field created by the circulating currents will add to the external field, slowly cancelling the average diamagnetic response of the device as one moves further away. Combining the two contributions, in the (finite) far field such a closed ring can be thus considered to be a weakly diamagnetic dipole. An array of these rings with radius r and lattice spacing a then exhibits on average a diamagnetic behavior, the strength of the effect proportional to the filling factor $F = \frac{\pi r^2}{a^2}$. This parameter is in fact the (area) density of the diamagnetic dipoles in the artificial homogenous medium. Nevertheless, due to the weak diamagnetic response of each individual SRR component in the array and the fact that $2r < a$, one can never obtain a large deviation of μ_{eff} from the free-space value μ_0 in such a case of closed-ring structures.

A split-ring structure is on the other hand magnetically more active as it exhibits resonant effects where the induced circulating currents can be essentially unbound in the case of zero ring resistance. The resonance effect is caused by the distributed $L-C$ interaction between the two rings, resulting in a very low series impedance in the equivalent circuit of the structure at resonance (see Figure 2 [1]). Since the resonant currents can be very large, the diamagnetic response from the structure is now much stronger than in the gapless case. If the rings are made of good conductors, the resonant series impedance is low and the diamagnetic response is very high. In the case of a superconductor with ideally

[1] The split-rings structure is in fact a circular coplanar transmission line operating in the even wave-propagation mode.

zero resistive loss, an SSRR array will - in the first order of approximation - have a negative infinite μ_{eff} at resonance (regardless of F). Evenmore, since the Q-factor will then also be infinite, the dispersion curve is discontinuous and the frequency selectivity is infinite as well. The response of the superconducting SRR is in practice limited by the resistance of the normal conducting charges, vortex-flow resistance and ultimately by the maximum supercurrent density J_c that the rings can carry. In any case, superconducting split-ring resonator arrays should offer a much better diamagnetic response when compared to arrays of normal-conducting elements.

We choose to implement the SSRR by using a high-T_c material (YBCO) suitable for use in liquid nitrogen for the purpose of reducing the cost and the complexity of the cryogenic environment. The structure we choose is square-shaped since it offers a slightly higher C for the same inductance L (the former proportional to the ring perimeter, the latter to the root of the area) than a circular shape, resulting in a lower resonance frequency. Figure 3 gives an overview of the structure and the steps necessary to manufacture it. Figure 4 is a photograph of an SSRR manufactured in our laboratory. The fundamental resonant frequency of the device is designed to be 3.6 GHz. Measurements are reported in the next section.

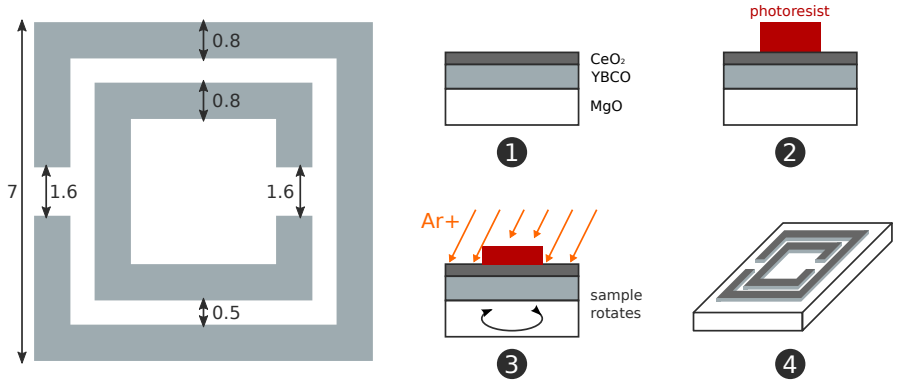

Figure 3: The dimensions of the SSRR in mm and the various manufacturing steps: 1) Base layers 2) Lithography for defining the SRR structure 3) Ar+ ion milling (with a rotating sample) etching the exposed areas 4) Final sample.

The epitaxial high-T_c YBCO film is 700 nm thick and grown on an MgO substrate[2]. The superconducting film has a transition temperature of around 87K and a critical current density of 2.4 MA/cm^2. The room temperature and sub-T_c electric loss tangents of MgO are $9 \cdot 10^3$ at 10 GHz [16] and $5 \cdot 10^6$ at 10.48 GHz [17], respectively. A capping isolating layer of 100 nm CeO_2 is used for protection of the sensitive YBCO top surface. These thin-film samples are commercially available in various sizes [3]. Sample production is currently restricted to an area of 3x3cm per day, this limitation stemming from the SSRR structuring process where the Ar+ ion-milling apparatus does not accept samples of

[2]Commercial supplier: THEVA Duennschichttechnik GmbH, Rote-Kreuz-Strae 8, D-85737 Ismaning

[3]One can obtain large substrates of up to 10 cm x 10 cm size and structure rings in a 2D array in a single process step if a suitable large-scale etching apparatus is available.

large size. If the individual SSRRs are about 1cm in diameter, the capacity thus stands at 9 SSRR/day. The SSRRs can at this point be manufactured with a very high yield (no defects in shape or thin-film microstructure).

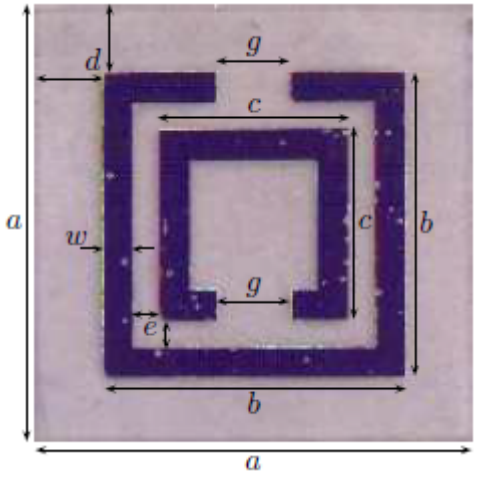

Figure 4: A photograph of a finished SSRR. Dimensions: a=10mm, b=7mm, c=4.4mm, d=1.5mm, e=0.5mm, g=1.6mm, w=0.8mm

3 Properties of SSRs

3.1 Measurement Setup

We measured the microwave properties of the SRR described above inside a WR-90 waveguide (see Figure 5). This waveguide type has an inner size of 22.86 mm ·10.16 mm, thus perfect for 10 mm ·10 mm samples. The usable frequency band of the wave-guide is 6.56 GHz (lower cutoff frequency) to 12.4 GHz (start of multiple waveguide modes). Since the basic resonance frequency of the SRR lies outside the usable frequency range of the WR-90, we operated the SRR in its first harmonic.

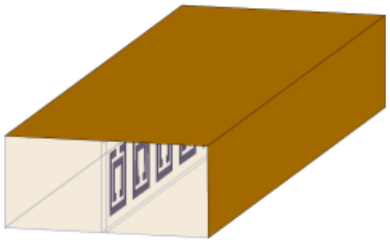

Figure 5: Schematic picture of the arrangement of samples inside the WR-90 waveguide

The waveguide environment was chosen for measurements because the waveguide components can easily be confined into a cryogenic enclosure and thus can

easily be temperature controlled and calibrated. A vacuum sealed cylindrical He flow-type cryostat (TRW) was used to confine and cool the waveguide components, which include two brass plated aluminum waveguide to 3.5 mm coaxial adapters and a 76.2 mm copper waveguide section holding the HTS SRR. The inner diameter of the cylinder is 74 mm, just wide enough to hold the waveguide components. Two holes were drilled at the top metal lid to allow the rigid steel coaxial cable to connect to the flexible coaxial cables that connect to a vector network analyzer (VNA). At the bottom of the cylinder, helium gas is allowed

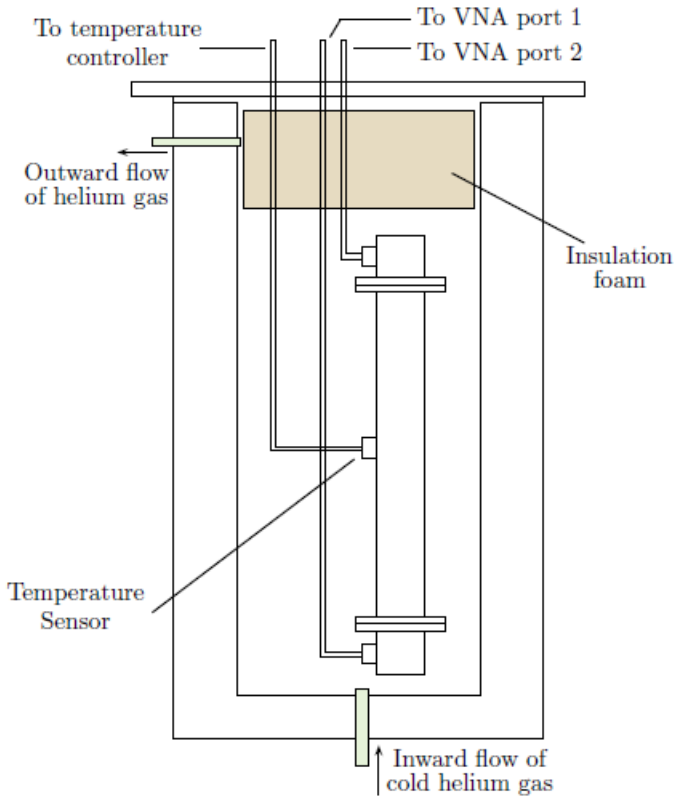

Figure 6: (a) A drawing of cryostat with waveguide components. (b) A photograph of the waveguide setup that fits inside the cryostat

Figure 7: A photograph of the measurement setup, showing the cryostat on top of a liquid helium filled dewar. To the right of the dewar are the VNA, flow control unit, and temperature controller.

to flow into the container to cool the whole structure. The temperature of the copper waveguide is monitored with an attached resistive sensor. Figure 6(a) shows the placement of the various components inside the cryostat along with the gas flow directions. Figure 6(b) shows a photograph of the waveguide unit that is placed in the cryostat. In the figure, one of the coaxial cable is twisted to the opposite side of the waveguide section to match the hole location on the cryostat lid.

The effects of wrapping the cable around the waveguide are removed through the calibration. Finally, the cryostat sits on top of a liquid helium filled dewar that supplies the cold helium gas to the waveguide components. Note that although liquid helium is used in this setup, liquid nitrogen could have been used instead since the T_c of YBCO is over 10 K higher than liquid nitrogen. A TRW flow control unit is used to control the flow of helium gas, thus controlling the temperature of the waveguide components, which is monitored by a LakeShore 330 autotuning temperature controller. This setup allows us to study the HTS SRR from room to sub-T_c temperature. A photograph of the whole measurement setup is shown in Figure 7.

3.2 Results: Quality Factor

At temperatures below T_c, one can see from the measurements in Figure 8 that the transmission resonances are sharp. This means that small sampling

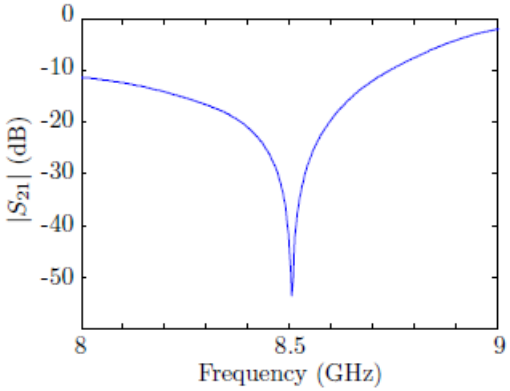

Figure 8: Measurement of the transmission resonance (S21) at 85 K. These resonances are sharp at sub-T_c temperatures.

frequency step size is needed to capture the exact resonance frequency, exact minimum S21, and 3 dB bandwidth for each resonance curve. However, due to the limitation of the measurement instruments, it is not possible to fully characterize these quantities. Therefore, a curve fitting method is utilized. The approach is to fit the data points (in dB and closed to the resonance) to a Lorentzian distribution and minimize the least square results. The Lorentzian function we are fitting to is

$$y(f) = A - \frac{1}{2\pi}\frac{B + C(f - f_0)}{(f - f_0)^2 + D^2}$$

where A, B, C, D, and f_0 are the fitting parameters. The term with a C multiple is included to factor in the asymmetry of the resonance curves. The parameters A, B, C, and D are only interesting in a sense where their values provide a good fit to our transmission curve. Fig. 9 shows the measured S21 data around the

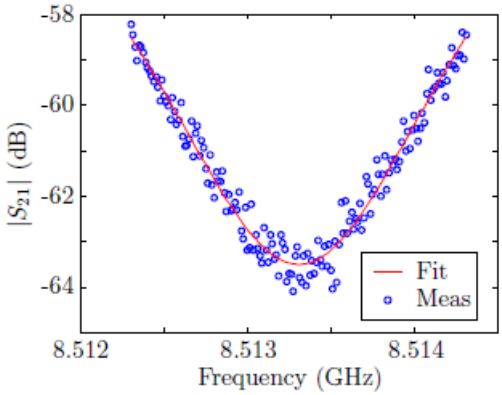

Figure 9: The circled points show the measured data for the lower of the two transmission resonances. The solid line is the Lorentzian curve fitted to the data.

8.513 GHz resonance at 81 K being fitted by this process. One can see that the measured data has unwanted noise and by relying on the minimum point, the resonance frequency and true minimum of S21 would be erroneously extracted.

The fitting process was applied to the measured transmission coefficients in the neighborhood of the resonance to give us an expression for the curve, from which the resonance frequency, minimum of S21, and 3 dB bandwidth can be obtained. The associated Q-factor is defined as $f_r/\Delta f_{3dB}$, where f_r is the resonance frequency and Δf_{3dB} is the 3 dB bandwidth. Thus, in Fig. 8, the fitted result (solid curve) gives f_r=8.5133 GHz, Δf_{3dB} = 1.36665 Mhz, and Q = 6230. The process is repeated for all other measured temperatures except for the 87 K data. This set of data did not fit the model and the Q factor has to be estimated, with Q≈42000. The plot of Q as a function of temperature is shown in Fig. 10.

For comparison, a copper SRR on a Rogers TMM10i substrate was fabricated and measured. This normal conducting SRR has Q=220, which is much lower than that of the HTS SRR when T<T_c.

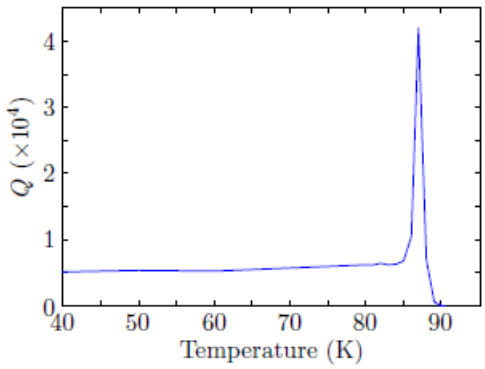

Figure 10: Quality factor vs temperature (K) for the measured HTS SRR inside a WR-90 waveguide. It peaks around 42000 at 87K and saturates around 5200.

We observe an unexpected spike in the quality factor (≈ 42000 at 87 K) which can be reproduced with different samples. This effect is unpredicted in simulations. Further experiments are under way to clarify the reason for this very high Q within a small temperature range.

3.3 Kinetic Inductance

The inductance of a superconducting SRR can be broken down to a geometric inductance (L_G) and a kinetic inductance (L_K). The geometric inductance is the conventional inductance of the SRR structure and is temperature independent. Its value can be estimated using the expression from Saha *et al.* [2].

$$L_G = 0.000508 l_{av} \left[2.303 \log_{10} \left(\frac{4 l_{av}}{w} \right) - 2.853 \right] (\mu H)$$

where, using the dimension in Fig. 4, $l_{av} = 4(b - 2w - e) - g$ is the average length of the strip in mm. We can approximate the SRR with a simple single

ring structure that has an effective radius r_m and the same L_G. The inductance of this simplified structure is approximated by [3].

$$\begin{aligned} L_G &= \frac{12.5\pi r_m}{8 + 11\frac{w}{r_m}} \times 10^{-6} \\ &= \gamma \mu_0 r_m \end{aligned}$$

where the effective radius of the ring, r_m, and line width, w, are in meters, and γ is the transform multiplier.

The kinetic inductance is known to be a function of the London penetration depth, which in turn depends on temperature, and can be approximated as [4]

$$\begin{aligned} L_K &\approx \mu_0 \frac{l}{w} \lambda \coth \frac{t}{\lambda} \\ &= \frac{\mu_0 2\pi r_m}{w} \lambda \coth \frac{t}{\lambda} \end{aligned}$$

where t is the thickness of the superconducting film and λ is the temperature dependent penetration depth, $\lambda(T) = \lambda(0)/\sqrt{1-(T/T_c)^2}$. Brorson *et al.* [5] estimated the absolute penetration depth $\lambda(0) = 148$ nm and Shi *et al.* [6] found $\lambda(0) = 198$ nm for $YBa_2Cu_3O_7$. There is still uncertainty pertaining to this value. Therefore, it will be one of the fitting parameters in fitting a theoretical model of the temperature dependence resonance frequency to the measurements.

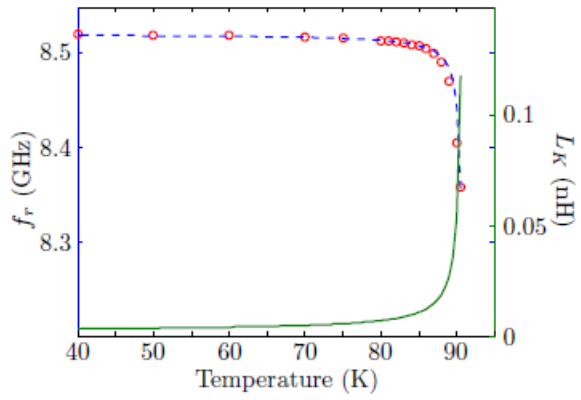

Figure 11: Resonance frequency vs temperature. The red circle line and blue dashed line represent measured and fitted resonance frequency, respectively, versus temperature. The green solid line is the calculated kinetic inductance vs temperature extracted from the fitting process.

The measured resonance frequency as function of the temperature for the SRR structure is shown in Figure 11, as the red circled points. As the temperature drops, we see an increase in the resonance frequency until it saturates. The main contribution to this effect is the kinetic inductance of the superconductor, which decreases with temperature. The fitting procedure is applied to

the measured data and the result is shown as the blue dashed line in Figure 11. From the fitted parameters, we can infer the following conclusions:

- $T_c = 91.27$ K. Above this temperature, the transmission resonances are not clearly defined. This value is close to the datasheet value. The difference can be attributed to the HTS film being slightly damaged.
- $f_G = 8.53$ GHz. This is the resonance frequency with the absence of the kinetic inductance.
- $\lambda(0) = 438$ nm. This is higher than published values of 148 nm [5] and 198 nm [6]. The damaged caused by the overexposure of the YBCO film during the photolithography process can contribute to this higher value.

Finally, the kinetic inductance versus temperature is shown as the solid green line in Figure 11. It shows the expected behavior, that L_K increases with temperature. This also means the total inductance (L_G+L_K) increases and thus lowers the resonance frequency. As can be seen, the kinetic inductance of this structure is very sensitive close to the T_c. One can make use of this property in the designs of microwave delay lines and kinetic inductance detectors mentioned earlier.

4 Tunable SSRR

Active superconducting circuits are typically based on the element of Josephson junction, a contact between two superconductting electrodes through an isolating or normal-metal barrier. The device supports a supercurrent flowing through the junction up to a given value, called the critical current I_C. The idea of a tunable superconducting resonator stems from the sensitivity of the critical current on the externally applied magnetic flux in the barrier

$$I_C = I_{C0} \cdot \frac{\sin\left(\frac{\pi\Phi_A}{\Phi_0}\right)}{\frac{\pi\Phi_A}{\Phi_0}} \tag{1}$$

where I_{C0} is the critical current in the absence of external field, Φ_A is the applied flux in the junction's barrier (direction normal to the supercurrent) and $\Phi_0 = 2.07\text{mV}\cdot\text{ps}$ is a constant named the magnetic flux quantum. Note that the applied magnetic field B_A giving rise to Φ_A in the junction is a contyrolling quantity that is seperately applied and should not be confused with the magnetic component of the EM wave B_{ext} travelling through the resonator. By changing the I_C with the applied field B_A through the Fraunhofer intereference pattern from (1), the properties of the supercurrent flow through the junction element change and one can thus extenally modulate the equivalent circuit seen between the terminals of said junction.

The $I - V$ characteristic of the junction is found by solving the RCSJ (Resistively and Capacitively Shunted Junction) set of equations:

$$I_J = I_C(\Phi_A) \cdot \sin(\varphi) + \frac{V_J}{R_J} + C_J \frac{dV_J}{dt} = I_S + I_R + I_C \tag{2}$$

$$V_J = \frac{\Phi_0}{2\pi} \frac{d\varphi}{dt} \tag{3}$$

where the phase φ (units of rad) has a physical meaning but can be treated as a help variable in our case. The currents I_R and I_C flow through the junction's parallel resistance R_J and capacitance C_J respectively, adding to the supercurrent component I_S. The voltage V_J across the terminals of the junction is, on the other hand, proportional to the derivative of the phase φ.

The supercurrent component $I_S = I_C(\Phi_A) \cdot \sin(\varphi)$ from the RCSJ model above behaves as a non-linear inductance. To see this, start from

$$\frac{dI_S}{dt} = I_C(\Phi_A) \cdot \cos(\varphi) \cdot \frac{d\varphi}{dt} \tag{4}$$

which, using the second expression from the RCSJ set, yields:

$$V_J = \frac{\Phi_0}{2\pi} \frac{1}{I_C(\Phi_A) \cdot \cos(\varphi)} \frac{dI_S}{dt} = L_J \frac{dI_S}{dt} \tag{5}$$

where $L_J(I_C, \varphi) = \frac{\Phi_0}{2\pi} \frac{1}{I_C(\Phi_A) \cdot \cos(\varphi)}$ is called the Josephson inductance. In the "small-signal" limit, i.e. when the amplitudes of the signals are small, L_J is linearazed in the vicinity of the operating point $\varphi \approx 0$ and one can then write:

$$L_{J0}(\Phi_A) = \frac{\Phi_0}{2\pi I_C(\Phi_A)} = \frac{\Phi_0}{2\pi I_{C0}} \cdot \left| \frac{\frac{\pi \Phi_A}{\Phi_0}}{\sin\left(\frac{\pi \Phi_A}{\Phi_0}\right)} \right| \tag{6}$$

where (1) was used. Note that the absolute sign in the relation above stems from the fact that φ changes by π when $I_C(\Phi_A)$ from equation (1) changes sign at $\Phi_A = n \cdot \Phi_0$ (this results from free-energy calculations). Hence, L_J is linearized at $\varphi \approx \pi$ instead of zero and the sign of L_{J0} stays positive.

It can be concluded that the Josephson inductance is modulated by the applied field in the junction barrier through the inverse-fraunhoffer pattern found in equation (6) above. The dependence is given in Figure 12 for a few values of the base critical current I_{C0}.

One must take care that the choice of I_{C0} is such that even when the ring is in resonance and hence carrying induced currents I_{ind} of high amplitudes, the junction - which is in series with the ring - can support them in the superconducting regime. A second problem is that even if we choose $|I_{ind}| < I_C(\Phi_A)$, the Josephson inductance can show non-linearity for induced amplitudes close to the critical current. This can give rise to distortion effects. Therefore, I_{C0} must be chosen as large as possible which, as seen from Figure 4, unfortunately results in a low value of L_J. Below a back-of-the-envelope estimation of the practicality of this tuning method is given.

4.1 Calculations single-junction tuning

Lets take, for example, the outer ring from Figure 2. The total series inductance of a ring of those dimensions can be estimated at approx. 10nH [7]. To achieve a change in the ring's L of at least 0.1% (=10pH), Figure 4 indicates to insert a junction (in series with the ring) with $I_{C0} < 500\mu$A - lets take $I_{C0} = 200\mu$A for this calculation.

Further, the induced RF currents circling the ring must be about 10% or less than I_{C0} in order for the Josephson inductance to behave roughly linearly.

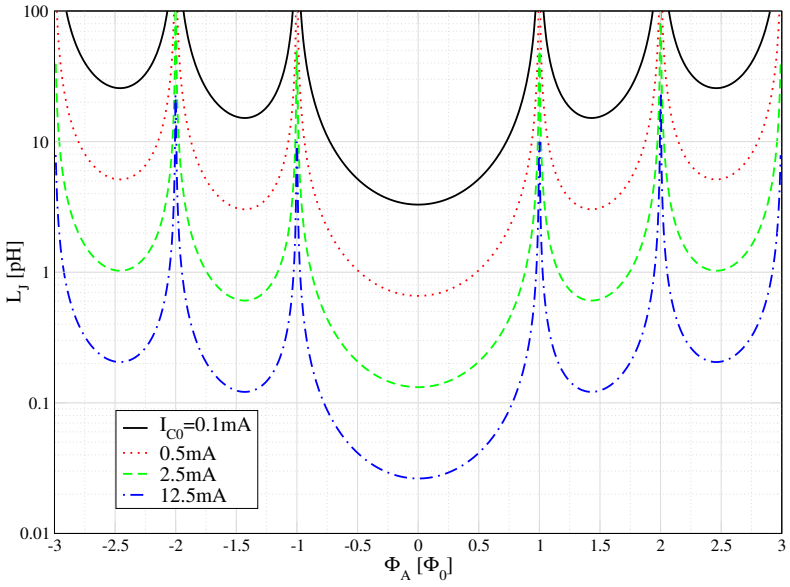

Figure 12: The Josephson inductance L_J around zero as a function of the magnetic flux applied in the junction's barrier for a few values of the base critical current I_{C0}. Note that although L_J diverges around $\Phi_A = n \cdot \Phi_0$, these points are characterised by a highly supressed I_C and hence impractical to use as modulation centerpoints

A current of amplitude 20μA flowing in a loop of approximately 3mm radius (our ring's size) gives a magnetic field (at the loop's center) of approximately 4nT ($B = \frac{\mu_0 I}{2R}$). Hence, our tunable ring can create a field with a maximum amplitude of about 4nT as a diamagnetic response to an incident field.

If one reduces the L of the rings and at the same time increases the mutual C by the same factor a, the resonance frequency will stay the same. The structure in Figure 5 replaces the coplanar coupling between the two rings with a microstrip type. The factor of increase in C per unit length, as compared to the coplanar type of same dimesions, can be calculated as

$$a = \frac{\epsilon_0 \frac{W}{d}}{\frac{\epsilon_0}{\pi} \ln\left(\frac{2W}{h}\right)} \tag{7}$$

Using $W = 0.8$mm, $h = 0.5$mm and $d = 200$nm, one obtains $a \approx 10^4$. In other words, if previously one used $L = 10$nH, it is now possible to achieve the same effect by using $L = 1$pH! Moreover, the (self)inductance of the rings is now exactly matched so that the structure has a higher symmetry and hence more order in its interaction with EM fields (and between the elements in an array). Lastly, the decreased size of the structure - while the resonance frequency and hence wavelength of the incident wave stay the same - makes it possible to populate an SSRR array with a higher relative spacing between the elements. This weakens the interaction between the elements in the array and reduces the influence of effects like the splitting of the resonance frequencies due to inter-element inductive coupling.

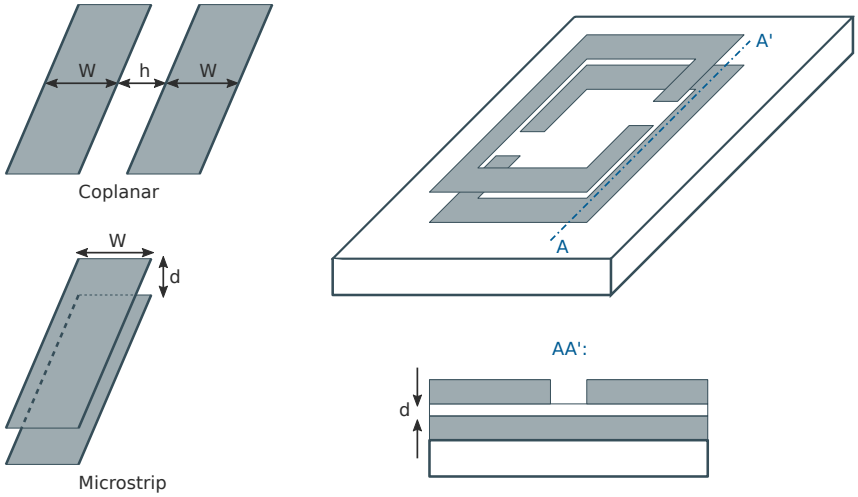

Figure 13: An microstrip SRR. The two films are deposited and structured independetly while the isolation layer is then deposited between those steps.

4.2 SQUID tuning

The idea is to use a two-junction interferometer device, a SQUID [8], instead of the single junction as a series tuning element in the ring. A drawing of an SSRR in this configuration is given in Figure 14.

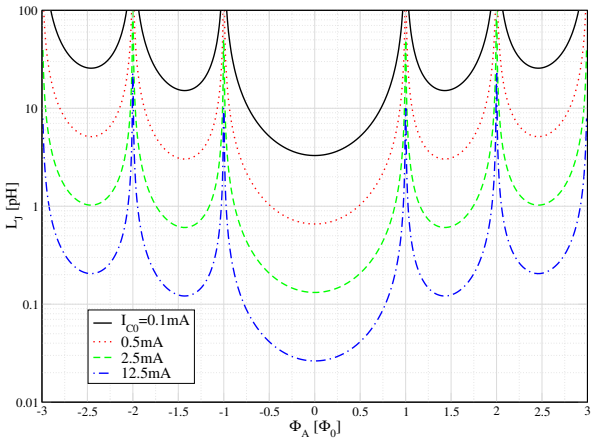

Figure 14: An SSRR with SQUID tuning. The substrate has a grain boundary aligned with the "gap" direction of the two rings. Creating two openings in the rings as givemn in the drawing would result in one SQUID in series with each ring.

When the parameters of the SQUID are such that $\beta_L = \frac{2\pi L I_C}{\Phi_0} << 1$, the element can be approximated as a composite Josephson junction of critical current

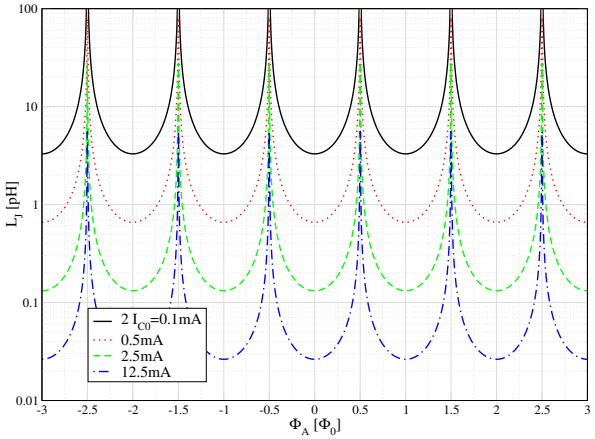

Figure 15: The Josephson inductance L_J of the SQUID around zero as a function of the magnetic flux applied to the device, for a few values of the total critical current $2I_{C0}$.

$$I_C(\Phi_A) = 2I_{C0} \cdot \cos\left(\pi \frac{\Phi_A}{\Phi_0}\right) \tag{8}$$

where I_{C0} is the critical current of each of the two junctions and the rest of the quantities have the same meaning as before. The Josepshon inductance is now

$$L_J(I_C) = \frac{\Phi_0}{2\pi(2I_{C0})} \frac{1}{\cos\left(\pi \frac{\Phi_A}{\Phi_0}\right)} \tag{9}$$

that is plotted in Figure 15.

4.3 Realization

It was planned to use the ramp-junction technique for the tuning Josephson junctions (see Figures 16 and 17). These junctions are very rigid, low inductance and capacitance and nicely scalable in their critical current. They require an elaboreate multilayer high-T_c process which the author developed for the University of Twente in the Netherlands. The base and top electrodes are made from DyBaCuO and the barrier from Ga-doped PrBaCuO layer. The whole process is fully epitaxial.

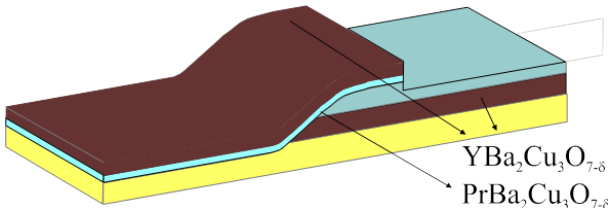

Figure 16: The ramp-type Josephson junction intended for magnetic tuning via Josephson inductance.

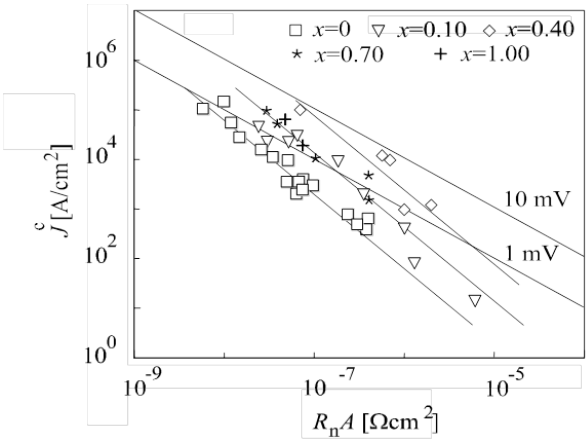

Figure 17: The critical current dependence on doping of the barrier and barrier thickness.

The unique preparation facilities for this junction type at the University of Twente became unavailable due to a move of the laboratory to a new location and due to new organizational structures in the Department. This part of the project is still going on. As junction types low-angle grain-boundary and implantation junctions are being evaluated. The most appropriate ones will be used in the next series of tunable SSRRs.

5 References

[1] J. Pendry, A. Holden, D. Robbins, and W. Stewart, Magnetism from conductors and enhanced nonlinear phenomena, IEEE Trans. Micr. Theory Tech., vol. 47, pp. 2075 2084, 1999.
[2] C. Saha and J. Y. Siddiqui, A comparative analyis for split ring resonators of different geometrical shapes, in Applied Electromagnetics Conference (AEMC), 2011 IEEE, dec. 2011, pp. 1 4.
[3] T. K. Ishii, Handbook of Microwave Technology. Academic Press, 1995, vol. 1.
[4] J. Pond, J. Claassen, and W. Carter, Kinetic inductance microstrip delay lines, Magnetics, IEEE Transactions on, vol. 23, no. 2, pp. 903 906, Mar. 1987.
[5] S. D. Brorson, R. Buhleier, J. O. White, I. E. Trofimov, H.-U. Habermeier, and J. Kuhl, Kinetic inductance and penetration depth of thin superconducting films measured by thz-pulse spectroscopy, Phys. Rev. B, vol. 49, pp. 61856187, Mar. 1994.
[6] L.-B. Shi, Y.-F. Wang, Y.-Y. Ke, G.-H. Zhang, S. Luo, X.-Q. Zhang, C.-G. Li, H. Li, and Y.-S. He, A study on the microwave responses of ybco and tbcco thin films by coplanar resonator technique, Chinese Physics, no. 10, pp. 30363041, Oct. 2007.
[7] see fig. 1 in Jaycox and Ketchen, IEEE Transactions on Magnetics vol.17 nr.1, 1981.

[8] For an overview see J.Clarke and A.I Braginski,The SQUID Handbook: Fundamentals and Technology of SQUIDs and SQUID Systems, Volume I and II, Wiley, 2005 and 2006.